Parametric image of myocardial blood flow generated from dynamic $H_2{}^{15}O$ PET using factor analysis and cluster analysis

J. S. Lee[1,2] D. S. Lee[1] J. Y. Ahn[1] G. J. Cheon[1] S.-K. Kim[1]
J. S. Yeo[1] K. S. Park[1,2] J.-K. Chung[1] M. C. Lee[1]

[1]Department of Nuclear Medicine, Seoul National University College of Medicine, Seoul, Korea
[2]Department of Biomedical Engineering, Seoul National University College of Medicine, Seoul, Korea

Abstract—*Algorithm-based parametric imaging of myocardial blood flow (MBF), as measured by $H_2{}^{15}O$ PET, has been the goal of many research efforts. A method for generating parametric images of regional MBF by factor and cluster analysis on $H_2{}^{15}O$ dynamic myocardial PET was validated by its comparison with gold-standard MBF values determined invasively using radiolabelled microspheres. Right and left ventricular blood pool activities and their factor images were obtained by the application of factor analysis to dynamic frames. By subtraction of the factor images multiplied by their corresponding values on the factors from the original dynamic images for each frame, pure tissue dynamic images were obtained, from which arterial blood activities were excluded. Cluster analysis that averaged pixels having time-activity curves with the same shape was applied to pure tissue images to generate parametric MBF images. The usefulness of this method for quantifying regional MBF was evaluated using canine experiment data. $H_2{}^{15}O$ PET scans and microsphere studies were performed on seven dogs at rest and after pharmacological stress. The image qualities and the contrast of parametric images obtained using the proposed method were significantly improved over either the tissue factor images or the parametric images obtained using a conventional method. Regional MBFs obtained using the proposed method correlated well with those obtained by the region of interest method ($r = 0.94$) and by the microsphere technique ($r = 0.90$). A non-invasive method is presented for generating parametric images of MBF from $H_2{}^{15}O$ PET, using factor and cluster analysis.*

Keywords—*PET, $H_2{}^{15}O$, Myocardial blood flow, Parametric image, Cluster analysis*

Med. Biol. Eng. Comput., 2005, **43**, 678–685

1 Introduction

DYNAMIC POSITRON emission tomography (PET) provides quantitative information on physiological processes. Water labelled with ^{15}O is a favourable radiopharmaceutical for the measurement of myocardial blood flow (MBF) using dynamic PET scans as it is metabolically inert, and its first-pass extraction across the myocardium is sufficiently high (BERGMANN *et al.*, 1984; ARAUJO *et al.*, 1991; LAMMERTSMA *et al.*, 1992; BOL *et al.*, 1993).

Because of its attractive and straightforward properties as a tracer for flow measurements, the kinetics of $H_2{}^{15}O$ can be described by a simple single-tissue compartment model. To estimate MBF using $H_2{}^{15}O$, however, the modelling equation for describing the kinetics of $H_2{}^{15}O$ in the myocardium should be modified to incorporate the correction parameters for partial volume and spillover effects, which are caused by the limited spatial resolution of the PET scanner and by the motion of the heart during the scanning period (HERRERO *et al.*, 1988; IIDA *et al.*, 1991; 2000).

Parametric imaging of MBF, obtained by the pixel-wise estimation of MBF, provides anatomically oriented information about the absolute MBF distribution without loss of spatial resolution and bias owing to the heterogeneity of MBF distribution that is generally associated with the region of interest (ROI) method (CHOI *et al.*, 1993; GEWIRTZ, 1993; CHEN *et al.*, 1998). The construction of an MBF parametric image from dynamic $H_2{}^{15}O$ PET is regarded as a challenging problem because of the high noise level in individual PET pixels and the complicated kinetic modelling equation required to describe the myocardial time–activity curves. The standard non-linear least squares (NLS) method frequently fails to generate an acceptable MBF parametric image with good statistical properties and image quality from $H_2{}^{15}O$ PET images.

Simplification methods have been suggested that involve the removal of the spillover term from the modelling equation using $C^{15}O$ blood pool scan data (IIDA *et al.*, 1988; 1991;

Correspondence should be addressed to Dr Kwang Suk Park; email: kspark@snuvh.snu.ac.kr

Paper received 11 November 2004 and in final form 6 April 2005
MBEC online number: 20054038

© IFMBE: 2005

2000). The assumptions about the venous fraction (fixed to 0.1 ml g^{-1}) used by these methods to simplify the parameter estimation procedures can be false under some physiological conditions (for example, under the hypertensive conditions induced by pharmacological stress, the venous fraction increased approximately three-fold) and thus can lead to erroneous MBF estimations. Other problems concerning the use of $C^{15}O$ PET, such as the incorrect estimation of MBF and related parameters, due to the misalignment of $H_2{}^{15}O$ and $C^{15}O$ PET images have also been acknowledged (IIDA *et al.*, 1988; 1991; 2000).

More recently, an alternative method of constructing the MBF parametric image has been suggested, and preliminary results have been reported (LEE *et al.*, 2000). In this method, factor analysis, a multivariate data analysis technique, was used to remove arterial blood pool activities from the myocardial dynamic PET images before the pixel-by-pixel parameter estimations were applied. This preprocessing procedure simplifies the model equation of tissue time–activity curves by eliminating the correction term for the spillover of arterial blood pool activity into the myocardium. Another important advantage of using factor analysis is the non-invasive determination of the arterial input function directly from the $H_2{}^{15}O$ dynamic PET image, without the acquisition of $C^{15}O$ data or the sampling of arterial blood (HERMANSEN *et al.*, 1998; AHN *et al.*, 2001). The simplified model equation with only two parameters was linearised, and cluster analysis (KIMURA *et al.*, 1999) was applied to the tissue time–activity curves to reduce the uncertainty in MBF estimation and the computation time required to generate the parametric images.

The aim of this study was to assess the reliability and possible limitations of the MBF parametric images generated by factor and cluster analysis. Thus we optimised the arterial input function by factor analysis (FA-based left ventricular (LV) input function) using the similarity between the FA-based LV input function and the LV input function as determined using the ROIs drawn on the centre of the LV cavity across multiple slices of myocardial factor images (ROI-based LV input function). Regional MBF values obtained from the parametric images using cluster analysis were then compared with those obtained using the conventional tissue ROI method and with those obtained using the MBF parametric images generated using the conventional NLS method. The parametric image method was also validated against 'gold standard' MBF values determined invasively using radiolabelled microspheres, which were simultaneously administered with $H_2{}^{15}O$ during PET scans.

2 Materials and methods

2.1 *O^{-15} water dog PET studies*

$H_2{}^{15}O$ PET scans were performed on seven dogs at rest ($n = 7$) and after pharmacological stress had been induced by adenosine or dipyridamole ($n = 5$). All scans were acquired with an ECAT EXACT 47 scanner*, which has an intrinsic resolution of 5.2 mm full width at half maximum (FWHM). Dynamic emission scans (5s × 12, 10s × 9, 30 × 3) were initiated simultaneously with the injection of 555–740 MBq $H_2{}^{15}O$, and these were continued for 4 min. Transaxial images were reconstructed using a filtered back-projection algorithm employing a Shepp–Logan filter with cutoff frequency of 0.3 cycles $pixel^{-1}$ as 128 × 128 × 47 matrices of size 2.1 × 2.1 × 3.4 mm. 'Principles of laboratory animal care (NIH publication 86-23)' were followed for all animal experiments.

*Siemens-CTI, Knoxville, TN, USA

2.2 *Microsphere studies*

Regional MBF was also measured using radiolabelled microspheres† of 15.5 μm diameter in six dogs at rest and in four dogs after stress induction, among the seven and five that underwent PET scans, respectively for each condition, and it was compared with the regional MBF obtained using PET images. After the dogs had been sacrificed, their hearts were removed and cut into 1 cm thick LV short-axis cross-sections, and the LV myocardium in each cross-section was further divided into four segments, namely, the anterior, lateral and inferior regions, and the septum. The regional MBF of each segment was then calculated using the standard microsphere reference technique (HEYMANN *et al.*, 1997; AHN *et al.*, 2001).

2.3 *Kinetic model*

The $H_2{}^{15}O$ tissue time–activity curve at time t (corrected for radiation decay) observed in the myocardial region can be described by the following equation (HERRERO *et al.*, 1988; IIDA *et al.*, 1991; 2000):

$$\begin{aligned} C_T(t) &= \alpha \cdot f \cdot C_a(t) \otimes e^{-(f/p)t} + V_a \cdot C_a(t) \\ &= K_1 \cdot C_a(t) \otimes e^{-k_2 t} + V_a \cdot C_a(t) \end{aligned} \quad (1)$$

where $\otimes$ denotes the convolution integral; $C_a(t)$ denotes the arterial blood input function; f denotes the myocardial blood flow free of the partial volume effect (MBF_p, ml min^{-1} g^{-1}); α denotes the perfusable tissue fraction (PTF, g ml^{-1}) or recovery coefficient; p denotes the partition coefficient of water (fixed at 0.91 ml g^{-1}); V_a denotes the arterial blood volume fraction (ml ml^{-1}); K_1 denotes the product of MBF_p and PTF (ml min^{-1} ml^{-1}, MBF_t); and k_2 denotes the quotient of MBF_p and the partition coefficient.

Conventionally, K_1, k_2, and V_a are estimated using NLS regression analysis, and MBF_p and PTF are computed using K_1 and k_2.

2.4 *Factor analysis of dynamic images*

To obtain factors and factor images from dynamic myocardial $H_2{}^{15}O$ PET images, we used a factor analysis method based on principal component analysis and followed this by oblique rotation of factor loadings, a method that was originally established by Barber and Di Paola *et al.* (BARBER, 1980; DI PAOLA *et al.*, 1982) and that was employed for extracting LV input functions and tissue time–activity curves from dynamic myocardial PET using $^{13}NH_3$ (WU *et al.*, 1995*a*), FDG (WU *et al.*, 1995*b*) or $H_2{}^{15}O$ (AHN *et al.*, 2001). We also determined the optimum scale factor to obtain the true LV input function from the LV factor (factor corresponding to the LV time–activity curve). The optimum scale factor was determined so that the scaled FA-based LV input function exhibited minimum deviation from the ROI-based LV input function.

The initial 18 frames (0–2 min) of the PET images were used for the factor analysis. The dynamic myocardial PET images were reoriented and re-sampled to produce short-axis images of 1 cm thickness to ensure the same orientation and slice thickness as used in the microsphere studies. We reoriented each dynamic image frame using the rotational and translational parameters determined for static images obtained by summing all of the dynamic frames. The linear interpolation method was used for re-sampling the reoriented images.

Only the cardiac regions were then masked, and the extracardiac components were removed to reduce the quantity of data

†NEN Life Science Products, Inc., Boston, MA, USA

and, hence, the burden of the calculation. The mask size was 32×32 (pixel $\times$ pixel), and the masked images were resized to 8×8 images to reduce statistical fluctuation (4×4 groups of pixels were averaged). The resulting masked images of dimensions $8 \times 8 \times 6 \times 18$ (pixel $\times$ pixel $\times$ plane $\times$ frame) were reformatted to 18×384 (frame $\times$ pixel) matrices for further analysis.

The underlying assumption behind the factor analysis was that the observable time–activity curve for each pixel in the PET images was equivalent to the weighted summation of the pure physiological factors, such as the RV and LV blood pool activity and the myocardial time–activity curves. The 384 reformatted time–activity curves of the pixels (dixels) in the mask were normalised and submitted for principal component analysis (PCA), to determine a low-dimensional subspace representing mainly relevant dixels. Oblique rotation of the basis vectors from the PCA was performed to obtain non-orthogonal basis vectors that represented factors with physical or physiological meaning. The iterative apex-seeking method suggested by Barber was used for oblique rotation (BARBER, 1980), instead of the user-interactive rotation of basis vectors used in our previous study (AHN *et al.*, 2001). Starting values for apex-seeking were selected using the method suggested by DI PAOLA *et al.* (1982).

Factor images were then computed by orthogonal projection of all dixels of the original masked dynamic images ($32 \times 32 \times 6 \times 18$ matrix) onto the determined factors (BARBER, 1980; DI PAOLA *et al.*, 1982). The number of factors was determined by visual assessment of factors and factor images. This strategy differs from that used in our previous study, in which the number of factors was fixed at three, as sometimes two or four factors produced better results (see Fig. 1; also refer to Section 4 for detail). As factor analysis produced only factors and factor images with obviously undesirable results (i.e. the mergence of LV blood pool and myocardial activity) when the assumed number of factors was incorrect, the determination of the number of factors by visual assessment was independent of observers and very reliable.

As each factor was in normalised units, the LV input function was obtained by rescaling of the LV factor, as performed by Wu *et al.* in their factor analysis of $^{13}NH_3$ and FDG PET data (WU *et al.*, 1995*a*; *b*). We used the average pixel value above a certain threshold in the LV factor image as a scale factor. The optimum threshold was determined by comparison of the rescaled LV factor with the ROI-based LV input function. The ROI-based LV input function was obtained from the original dynamic images using small circular ROIs ($\sim$100 mm^2), which were small enough to avoid any spillover contamination due to myocardium activity. The small ROIs drawn on the centre of the LV cavities in the myocardium factor images were copied onto the original dynamic images to obtain the LV time–activity curves, and the time–activity curves from two ROIs on two neighbouring mid-ventricular slices were averaged to reduce statistical noise.

We varied the threshold used to rescale the LV factor in increments of 5% over the range 30–95% of the maximum pixel value in the LV factor image and computed the relative errors of the areas under the curves of the LV factors scaled using the various thresholds against the ROI-based LV input function; we then selected an optimum threshold that minimised the average relative error.

2.5 *Generation of parametric images using cluster analysis*

To obtain the dynamic tissue image in which arterial blood components were excluded in each frame, RV and LV factor images were multiplied by their corresponding RV and LV factors and then subtracted from the original dynamic images. This procedure can be written as

$$I_{tissue}(t_i) = I_{original}(t_i) - [FI_{RV} \times f_{RV}(t_i) + FI_{LV} \times f_{LV}(t_i)] \quad (2)$$

where $I_{tissue}(t_i)$ is the pure tissue image at t_i, where $t_i = t_1, t_2, \ldots, t_n$ are the sampling times of the PET measurements; $I_{original}$ (t_i) is the original dynamic image at t_i; FI_{RV} and FI_{LV} are RV and LV factor images; and f_{RV} (t_i) and f_{LV} (t_i) are the amplitudes of the RV and LV factors at t_i.

Although the RV and LV factors are in normalised units (the norm of each factor equalled to 1.0), each pixel value of the factor image can be regarded as the weight for the corresponding factor to compose the original time–activity curve in that pixel. Therefore RV and LV factors were not specially scaled for this subtraction, unlike the determination of the input function.

By the removal of these arterial blood pool activities from the original dynamic images, the correction terms representing spillover effect ($V_a \cdot C_a(t)$) can be omitted from the kinetic modelling equation (1) of the myocardial time–activity curve. Thus the modelling equation was simplified sufficiently to allow the cluster analysis specified in the Appendix to be used, which involved the estimation of only two parameters (K_1 and k_2).

The parametric images of MBF_t (K_1) and PTF ($K_1/k_2 \times p$) were then composed using the optimised FA-based LV input

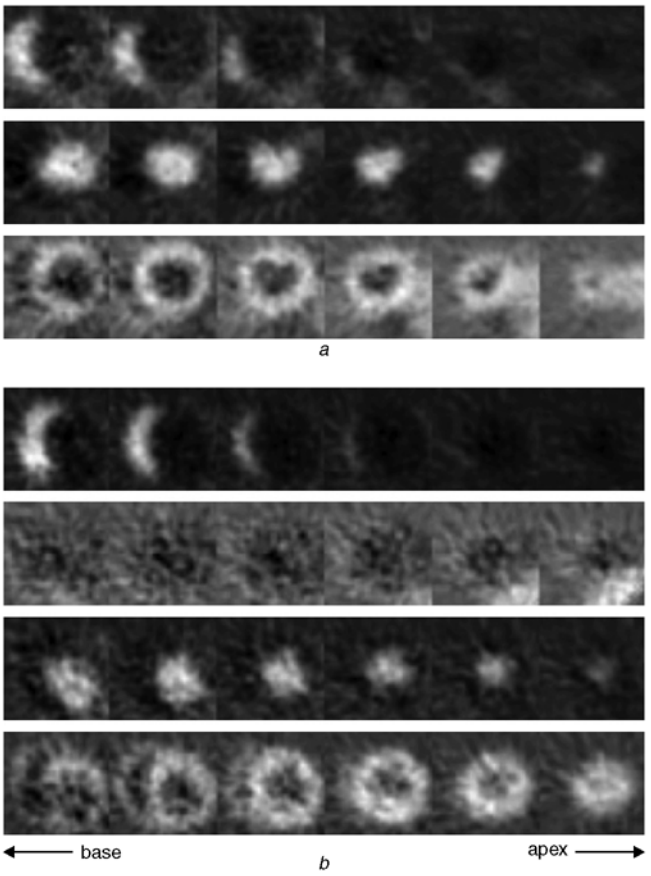

Fig. 1 *Factor images obtained from dynamic $H_2{}^{15}O$ PET study in canine model. (a) Three factor images, right ventricle (upper), left ventricle (middle) and myocardium (lower), obtained from PET image at rest. (b) Factor images obtained from PET study during pharmacological vasodilator stress. Hepatic activity (second row) was separated from myocardial activity (fourth row)*

function. As pixels that have similar ratios of the first and zeroth moments of the tissue time–activity curve have similar k_2 and thus similar shapes, pixels were grouped into classes (i.e. clusters) according to the ratios of these moments. Clustering size was 100 pixels a cluster. K_1 and k_2 for each cluster were estimated using linear least squares curve-fitting (FENG *et al.*, 1993; 1996). K_1 for individual pixels was obtained by multiplying the K_1 of a cluster by the ratio of the zeroth moments of each pixel and cluster (KIMURA *et al.*, 1999) (see Appendix for further details).

To allow comparisons with the conventional method, parametric images of MBF_t and PTF were also generated using the three-parameter NLS method, which enabled the determination of three parameters (K_1, k_2, and V_a), and the two-parameter (K_1 and k_2) NLS method performed on the dynamic tissue images with the RV and LV components removed (Equation 2).

2.6 *Comparison with other methods*

Polygonal ROIs were drawn on the myocardium factor images. Four segments of the anterior, lateral and inferior regions and of the septum were determined in the same way as performed in the microsphere studies. The ROIs were then copied onto the original dynamic images to produce tissue time–activity curves, and onto the MBF_t and PTF parametric images to produce the mean MBF_t and PTF values for each ROI. The regional MBF_p (the myocardial blood flow free of partial volume effect) value for each ROI was then calculated using the ratio of the mean MBF_t and PTF values.

Regional MBF_p values obtained using the parametric images were compared with the microsphere MBF values and with the MBF_p values obtained using the conventional ROI method, in which the average tissue time–activity curve for each tissue ROI and FA-based input function were used to fit (1).

2.7 *Statistical analysis*

Correlation coefficients of the MBFs obtained using the different methods were computed. Mean differences between paired measurements (parametric image minus ROI method or microsphere) were shown on a Bland–Altman plot, and two SDs of the differences were calculated.

3 Results

3.1 *Factor analysis*

In all cases, factors and their factor images were obtained successfully. In the $H_2{}^{15}O$ PET images acquired in the rest state, three factors corresponding to RV, LV and myocardium time–activity curves were obtained from six of the seven dogs. In the remaining dog, only two factors were obtained, as the RV and LV time–activity curves were not separated. Fig. 1*a* shows three factor images obtained from a dog PET image at rest. In the factor images, RV and LV blood pool activities were separated from myocardial activity, but the myocardium factor image included hepatic activity at the apex region of the heart. Increasing the number of factors did not improve the separation of myocardial activity from hepatic activity.

Of the images taken following adenosine or dipyridamole stress, three factors were obtained from three of the five dogs. In one dog, only two factors were obtained, as the RV and LV time–activity curves were not separated, and, in the remaining dog, four factors were obtained. Fig. 1*b* shows the factor images of the latter case. Hepatic activity (the second row) was separated from myocardial activity (the fourth row).

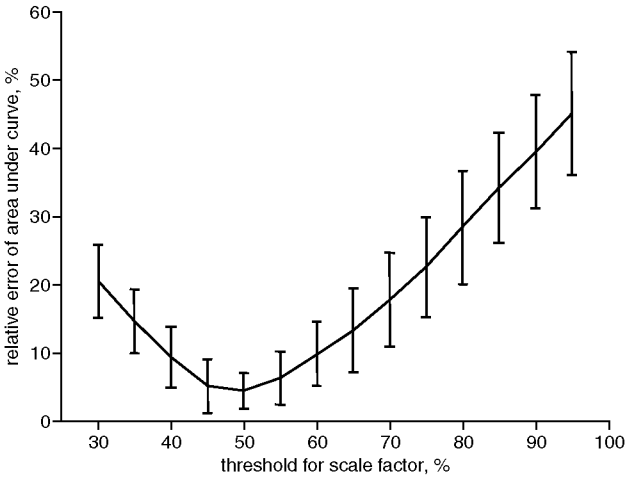

Fig. 2 *Mean and standard deviations of relative errors between areas under curves of scaled LV factor and ROI-based LV input function as function of threshold*

3.2 *Scale factor of the FA-based LV input function*

The optimum threshold required to rescale the LV factor to obtain the FA-based LV input function was 50% of the maximum pixel value in the LV factor image. The mean and standard deviation (SD) of the relative errors between the areas under the curves of the scaled LV factor and of the ROI-based LV input function as a function of threshold are shown in Fig. 2. At 50% of the maximum pixel value, the relative error was at a minimum and most stable (mean error = 4.3 ± 2.7%). The FA-based LV input function scaled with 50% thresholds was similar to the ROI-based LV input function (Fig. 3). The FA-based LV input function showed slightly lower peak activity and slightly greater dispersion around the initial peak than the ROI-based LV input function. Regional MBF_p values obtained using ROI-based and FA-based LV input functions were strongly correlated ($y = 1.10x + 0.27$, $r = 0.98$, x: ROI-based input function) when the MBF_p values were estimated using the ROI-based tissue time–activity curves and NLS method.

3.3 *MBF parametric image*

Fig. 4 shows the parametric images of MBF_t (Fig. 4*a*) and PTF (Fig. 4*b*) obtained using the FA-based input

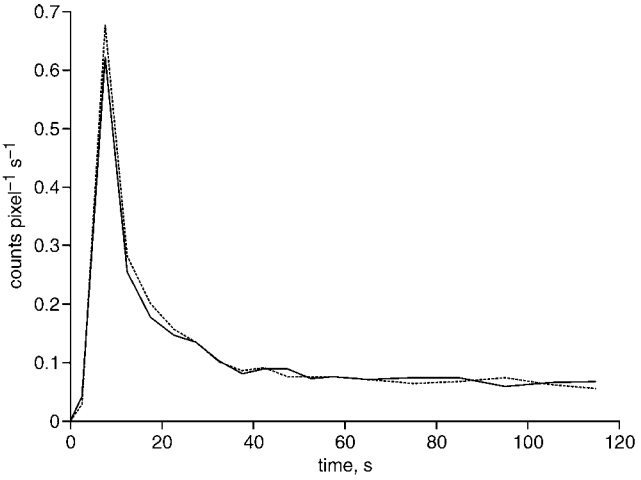

Fig. 3 *(—) LV factor scaled with 50% thresholds and (...) ROI-based LV input function obtained using small ROIs drawn at centre of LV cavity*

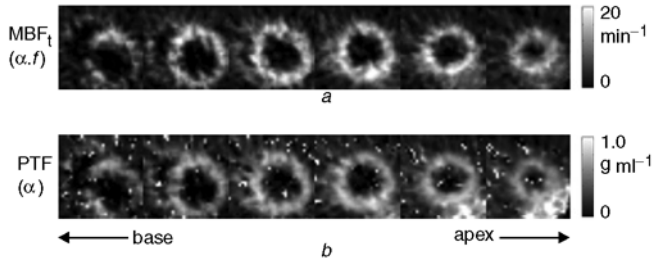

Fig. 4 *Parametric images of (a) MBF$_t$ and (b) PTF using factor and cluster analysis*

function and cluster analysis. These parametric images showed better image quality and contrast than the factor image of the myocardium and parametric images obtained using the NLS methods (Fig. 5); this result was consistent in all dog studies.

Regional MBF$_p$ obtained from parametric images using cluster analysis showed a good correlation ($y = 0.84x + 0.82$, $r = 0.94$) with that obtained using the conventional ROI method, in which the MBF$_p$s were obtained using an average time–activity curve for each tissue ROI and FA-based LV input function, as shown in Fig. 6*a*. Regression analysis showed relatively poorer slope value and systemic error in the septum ($y = 0.80x + 1.04$) in comparison with the other regions (anterior wall: $y = 0.88x + 0.59$; inferior: $y = 0.89x + 0.72$; lateral: $y = 0.81x + 0.94$). PTF values obtained using both methods were well correlated ($y = 0.85x + 0.04$, $r = 0.85$).

A good correlation was also obtained between the regional MBF$_p$s of parametric images obtained using cluster analysis and the MBFs obtained using the microsphere method ($y = 0.94x + 0.85$, $r = 0.90$), as shown in Fig. 6*c*. The Bland–Altman plots (Figs 6*b* and *d*) showed neither proportional error nor an increase in variability of the differences as the magnitude of the MBF$_p$ values increased. However, there was a consistent systemic bias in the parametric image-determined MBF$_p$ with respect to the ROI- and microsphere-determined values. Relatively large deviation between the methods (~100% spread of data to 2SD in rest flow range) was also observed. Bland–Altman plots between parametric image- and microsphere-determined MBF$_p$ values for individual anatomical regions of interest showed that the systemic bias in parametric image-determined MBF$_p$ was lowest in the inferior territory (0.35 ml min^{-1} g^{-1}) and highest in the septum (0.94 ml min^{-1} g^{-1}). However, the variability of the differences was smallest in the septum.

Regional analysis for each dog and condition showed that parametric image-determined MBF$_p$ was homogeneous throughout the myocardium. The mean coefficient of variation was 11.6%, which was comparable with previously reported values obtained using the ROI method (ARAUJO *et al.*, 1991).

On the other hand, the MBF$_p$ obtained from parametric images using the three-parameter NLS method was overestimated and exceeded physiologically relevant values in some cases.

Using IDL[‡] language, the computation time required to generate parametric images using factor and cluster analysis was about 0.2 s for a $32 \times 32 \times 6 \times 18$ (pixel × pixel × plane × frame) matrix on a personal computer fitted with a 850 MHz Pentium III CPU and 768 MB of memory, whereas the three-parameter NLS method required more than 4 min.

[‡]Research Systems Inc., Boulder, CO, USA

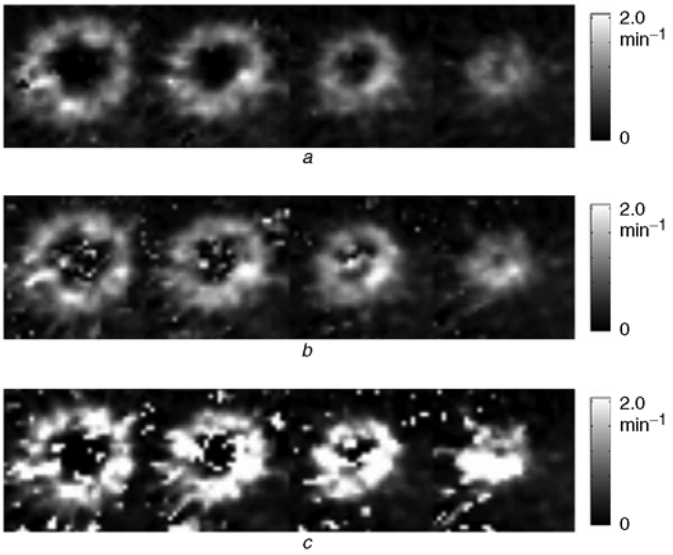

Fig. 5 *Comparison of parametric images of MBF$_t$ obtained using (a) cluster analysis + two-parameter LLS, (b) two-parameter NLS and (c) three-parameter LLS*

4 Discussion

A method for composing parametric images of regional cerebral blood flow (CBF) was suggested by KIMURA *et al.* (1999), in which the signal-to-noise ratio (SNR) of the parametric image was improved and computation time was reduced by the application of cluster analysis to the tissue time–activity curves. However, there was an obstacle in the application of this method to the composition of the parametric image of MBF as measured by $H_2{}^{15}O$ PET, namely, that the kinetic modelling equation for the tissue time–activity curve is not as simple as that of CBF, as the time–activity curve of the myocardium is contaminated by ventricular blood pool activity. Although this spillover effect can be corrected for by its inclusion as a parameter in the kinetic equation, the correction parameter makes the modelling equation more complex and prevents the application of the Kimura cluster analysis to the MBF parametric image.

In this study, factor analysis was used to overcome this obstacle. The spillover effect was removed by extraction of the RV and LV blood pool time–activity curves and their factor images and by subtraction of the factor images multiplied by their corresponding factors from the original dynamic images. The MBF parametric image was then composed by cluster analysis using the FA-based LV input function and pure tissue time–activity curves from which arterial blood pool activities were excluded. The need for an additional $C^{15}O$ scan and the possible accompanying errors due to the use of $C^{15}O$ data were also eliminated by the use of factor analysis. We obtained the LV input function directly from $H_2{}^{15}O$ dynamic PET without $C^{15}O$ data or arterial blood sampling.

In the present study, in which $H_2{}^{15}O$ was administered by bolus injection with a short injection time, RV and LV activities were separated by factor analysis in six out of seven cases at rest and in four out of five cases after the application of stress. The RV and LV factors exhibited different peak activity times, and the LV factors showed a broader width than the RV factors owing to greater dispersion.

Two images, from which RV and LV activities were not separated by the factor analysis, were obtained from the same dog. In the PET experiments on this dog, although the injection duration was no longer than that used in other studies, the PET images obtained were of a poorer image quality owing to the lower activity of the injected $H_2{}^{15}O$.

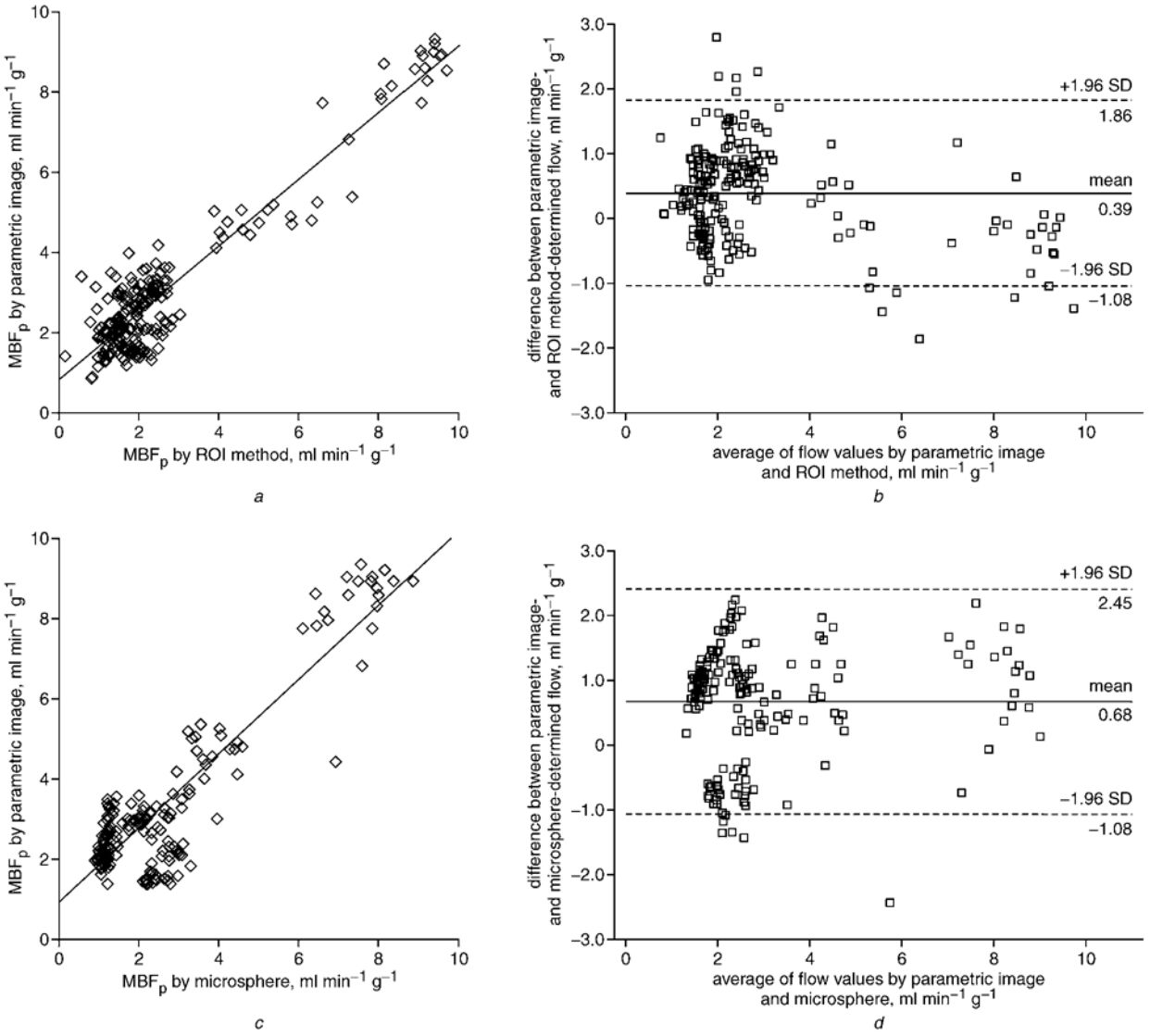

Fig. 6 *Comparison of MBF_p values obtained from parametric image using factor and cluster analysis with those obtained using ROI and microsphere methods. (a) Correlation between parametric image and ROI determined MBF_p values ($y = 0.84x + 0.82$, $r = 0.94$). (b) Difference between parametric image- and ROI-determined MBF_p values plotted against averages of two measurements (Bland–Altman plot). (c) Correlation between parametric image- and microsphere-determined MBF_p values ($y = 0.94x + 0.85$, $r = 0.90$). (d) Bland–Altman plot between parametric image- and microsphere-determined MBF_p values*

This female dog also had a relatively small heart; the RV cavity was particularly small on factor images. In view of the above, the RV and LV activities were not separated by factor analysis in this animal because of the relatively small contribution made by RV activity to the PET count variation compared with the level of statistical noise.

In most cases, liver activity appeared in the myocardium factor images, and these activities were not separated from each other, although we increased the assumed number of factors. MBF at rest is similar to, or slightly higher than, hepatic blood flow (PETERS and MYERS, 1998), but the difference between MBF and hepatic blood flow increases under the hypotensive conditions induced by adenosine or dipyridamole stress (BOARINI *et al.*, 1982; KASSELL *et al.*, 1983). As time–activity curves at higher blood flow have a steeper slope during both the build-up and washout phases, the time–activity curve at increased MBF has a different shape from the liver time–activity curve. Therefore factor analysis is expected to be able to distinguish between these two different components in dynamic PET images under conditions of pharmacological stress. In fact, myocardial activity was separated from liver activity when MBF after stress was high enough (Fig. 1*b*). The dog that produced the image shown in Fig. 1*b* had the highest MBF value (mean MBF: 7.4 ml min^{-1} g^{-1}) in this study.

As we used factor analysis for preprocessing before generating the MBF parametric image by cluster analysis, the accuracy of the MBF estimation is dependent on the result of the factor analysis. The use of factor analysis for the quantification of MBF using $H_2{}^{15}O$ PET has already been validated in terms of its accuracy, but it is known that the MBF is slightly overestimated in comparison with that obtained by the microsphere technique if physiological factors are not completely separated (AHN *et al.*, 2001).

In the present study, the effects of such incomplete separation of physiological factors, owing to ambiguities in the determination of a unique solution by factor analysis, may be more substantial than indicated by the previous study, as we derived both the arterial blood volume fraction for each pixel and the LV input function by factor analysis. The contamination of the LV input function by the spillover of myocardial activity disperses the LV input function, and contamination in the reverse direction results in a steeper slope during both the build-up and washout phases of the tissue time–activity curve. These bidirectional contaminations contribute to an increase in the estimated MBF: the slight

off-zero y-intercepts in the regression lines (Fig. 6) may be explained in part by these bidirectional activity contaminations. More investigation of systemic bias in MBF, which was apparent particularly in the low MBF range, using an animal model of myocardial ischaemia and infarction by coronary occlusion would be valuable.

Considerable deviation between the rest MBF values obtained by the different methods was also observed in the Bland–Altman plots (Fig. 6), suggesting a possible limitation of this parametric imaging method for the assessment of subtle MBF abnormality. This deviation could subsume the uncertainty in the radiation detection process in PET and gamma counter systems, errors in flow measurement by both the $H_2{}^{15}O$ PET and microsphere techniques, and imperfect match of the myocardial sub-regions.

More investigations into methodological improvements are warranted to minimise the errors in MBF estimates by the parametric image, which were propagated from all the processing steps including factor analysis, cluster analysis and tracer kinetic modelling. Although high noise levels and the finite time resolution of dynamic $H_2{}^{15}O$ PET scans limit the perfect separation of factors, a greater level of sophistication in the data analysis method with the relevant physiological and physical constraints on dynamic PET data should improve the performance of the factor extraction (LEE *et al.*, 2001*a*; *b*; SITEK *et al.*, 2002). Investigations into one-step approaches for parametric image generation, which simultaneously determine the three parameters, including the arterial blood volume fraction, represent an approach from another direction that could improve MBF parametric imaging (IIDA *et al.*, 1988; KIMURA *et al.*, 2002; LEE *et al.*, 2001*c*).

More investigation into the feasibility of the proposed approach for measurements of blood flow in the more complex setting of the human heart would also be required, as the image quality tends to be much better in dogs than in humans owing to significantly more attenuation of photons in humans. Improved multivariate analysis techniques in human cardiac component separation from $H_2{}^{15}O$ PET data would be useful for increasing the feasibility of the present approach in human data analysis (LEE *et al.*, 2005).

Appendix

Cluster analysis

If the tissue time–activity curve is free from the 'spillover' effect, (1) can be simplified to the following:

$$C(t) = K_1 \cdot C_a(t) \otimes e^{-k_2 t} \tag{3}$$

Then, the ratio of the first and the zeroth moments of the tissue time–activity curve R can be expressed as

$$R = \frac{M_1}{M_0} = \frac{\int_0^T t \cdot C(t)\,dt}{\int_0^T C(t)\,dt} = \frac{\int_0^T t \cdot C_a(t) \otimes e^{-k_2 t}}{\int_0^T C_a(t) \otimes e^{-k_2 t}} = f(k_2) \tag{4}$$

It can be seen that the ratio R is a function of only k_2. The ratio R is actually a monotonic decreasing function of k_2 within the physiological range of k_2 (KIMURA *et al.*, 1999). This means that pixels that have a similar R have a similar k_2. The idea of cluster analysis is to average the time–activity curves with similar k_2 by grouping them according to the ratio R.

Then, the average time–activity curve for a cluster is expressed by the following:

$$\overline{C^{(i)}(t)} = \overline{K_1^{(i)}} \cdot C_a(t) \otimes e^{-k_2^{(i)} t} \tag{5}$$

where $\overline{K_1^{(i)}}$ is the average K_1 in this cluster. The average K_1 and the k_2 can be estimated by least squares fitting to this equation.

K_1 for individual pixels can be obtained by multiplication of the average K_1 of the cluser by the ratio of the zeroth moment between the pixel and the cluster, as determined by

$$K_1^{(ij)} = \overline{K_1^{(i)}} \frac{M_0^{(ij)}}{M_0^{(i)}} \tag{6}$$

The image quality and the accuracy of the parameter estimation would be increased by using this method, as parameters are estimated from the averaged tissue time–activity curves. Fast computation is also possible because the parameter estimation is repeated only once per cluster, and because the computation of individual K_1s is a simple arithmetic operation (KIMURA *et al.*, 1999).

Acknowledgments—The authors would like to thank Dr Hideiro Iida at the National Cardiovascular Center Research Institute, Osaka, and Dr Yuichi Kimura at the Tokyo Metropolitan Institute of Gerontology, for their valuable comments and helpful discussions.

This work was supported in part by the Korean Ministry of Science & Technology and by the Brain Korea 21 Human Life Sciences program.

References

AHN, J. Y., LEE, D. S., LEE, J. S., KIM, S. K., CHEON, G. J., YEO, J. S., SHIN, S. A., CHUNG, J. K., and LEE, M. C. (2001): 'Quantification of regional myocardial blood flow using dynamic $H_2{}^{15}O$ PET and factor analysis', *J. Nucl. Med.*, **42**, pp. 782–787

ARAUJO, L. I., LAMMERTSMA, A. A., RHODES, C. G., MCFALLS, E. O., IIDA, H., RECHAVIA, E., GALASSI, A., DE SILVA, R., JONES, T., and MASERI, A. (1991): 'Noninvasive quantification of regional myocardial blood flow in coronary artery disease with oxygen-15-labeled carbon dioxide inhalation and positron emission tomography', *Circulation*, **83**, pp. 875–885

BARBER, D. C. (1980): 'The use of principal components in the quantitative analysis of gamma camera dynamic studies', *Phys. Med. Biol.*, **25**, pp. 283–292

BERGMANN, S. R., FOX, K. A., RAND, A. L., MCELVANY, K. D., WELCH, M. J., MARKHAM, J., and SOBEL, B. E. (1984): 'Quantification of regional myocardial blood flow in vivo with $H_2{}^{15}O$', *Circulation*, **70**, pp. 724–733

BOARINI, D. J., KASSELL, N. F., OLIN, J. J., and SPROWELL, J. A. (1982): 'The effect of intravenous dipyridamole on the cerebral and systemic circulations of the dog', *Stroke*, **13**, pp. 842–847

BOL, A., MELIN, J. A., VANOVERSCHELDE, J. L., BAUDHUIN, T., VOGELAERS, D., DE PAUW, M., MICHEL, C., LUXEN, A., LABAR, D., COGNEAU, M. *et al.* (1993): 'Direct comparison of [^{13}N]ammonia and [^{15}O]water estimates of perfusion with quantification of regional myocardial blood flow by microspheres', *Circulation*, **87**, pp. 512–525

CHEN, K., LAWSON, M., REIMAN, E., COOPER, A., FENG, D., HUANG, S. C., BANDY, D., HO, D., YUN, L. S., and PALANT, A. (1998): 'Generalized linear least squares method for fast generation of myocardial blood flow parametric images with N-13 ammonia PET', *IEEE Trans. Med. Imaging*, **17**, pp. 236–243

CHOI, Y., HUANG, S. C., HAWKINS, R. A., KUHLE, W. G., DAHLBOM, M., HOH, C. K., CZERNIN, J., PHELPS, M. E., and SCHELBERT, H. R. (1993): 'A simplified method for quantification of myocardial blood flow using nitrogen-13-ammonia and dynamic PET', *J. Nucl. Med.*, **34**, pp. 488–497

DI PAOLA, R., BAZIN, J. P., AUBRY, F., AURENGO, A., CAVAILLOLES, F., HERRY, J. Y., and KAHN, E. (1982): 'Handling of dynamic sequences in nuclear medicine', *IEEE Trans. Nucl. Sci.*, **29**, pp. 1310–1321

FENG, D., WANG, Z., and HUANG, S.-C. (1993): 'A study on statistically reliable and computationally efficient algorithms for generating local cerebral blood flow parametric images with positron emission tomography', *IEEE Trans. Med. Imaging*, **12**, pp. 182–188

FENG, D., HUANG, S.-C., WANG, Z., and HO, D. (1996): 'An unbiased parametric imaging algorithm for nonuniformly sampled biomedical system parameter estimation', *IEEE Trans. Med. Imaging*, **15**, pp. 512–518

GEWIRTZ, H. (1993): 'Parametric images for quantitative measurements of regional myocardial blood flow in humans: a step in the right direction', *J. Nucl. Med.*, **34**, pp. 862–864

HERMANSEN, F., ASHBURNER, J., SPINKS, T. J., KOONER, J. S., CAMICI, P. G., and LAMMERTSMA, A. A. (1998): 'Generation of myocardial factor images directly from the dynamic oxygen-15-water scan without use of an oxygen-15-carbon monoxide blood-pool scan', *J. Nucl. Med.*, **29**, pp. 1696–1702

HERRERO, P., MARKHAM, J., MYEARS, D. W., WEIHEIMER, C. J., and BERGMANN, S. R. (1988): 'Measurement of myocardial blood flow with positron emission tomography: correction for count spillover and partial volume effects', *Math. Comput. Model.*, **11**, pp. 807–812

HEYMANN, M. A., PAYNE, B. D., HOFFMAN, J. I., and RUDOLPH, A. M. (1977): 'Blood flow measurements with radionuclide-labeled particles', *Prog. Cardiovasc. Dis.*, **20**, pp. 55–79

IIDA, H., KANNO, I., TAKAHASHI, A., MIURA, S., MURAKAMI, M., TAKAHASHI, K., ONO, Y., SHISHIDO, F., INUGAMI, A., and TOMURA, N. (1988): 'Measurement of absolute myocardial blood flow with $H_2{}^{15}O$ and dynamic positron-emission tomography. Strategy for quantification in relation to the partial-volume effect', *Circulation*, **78**, pp. 104–115

IIDA, H., RHODES, C. G., DE SILVA, R., YAMAMOTO, Y., ARAUJO, L. I., MASERI, A., and JONES, T. (1991): 'Myocardial tissue fraction–correction for partial volume effects and measure of tissue viability', *J. Nucl. Med.*, **32**, pp. 2169–2175

IIDA, H., TAMURA, Y., KITAMURA, K., BLOOMFIELD, P. M., EBERL, S., and ONO, Y. (2000): 'Histochemical correlates of ^{15}O-water-perfusable tissue fraction in experimental canine studies of old myocardial infarction', *J. Nucl. Med.*, **41**, pp. 1737–1745

KASSELL, N. F., BOARINI, D. J., OLIN, J. J., and SPROWELL, J. A. (1983): 'Cerebral and systemic circulatory effects of arterial hypotension induced by adenosine', *J. Neurosurg.*, **58**, pp. 69–76

KIMURA, Y., HSU, H., TOYAMA, H., SENDA, M., and ALPERT, N. M. (1999): 'Improved signal-to-noise ratio in parametric images by cluster analysis', *Neuroimage*, **9**, pp. 554–561

KIMURA, Y., SENDA, M., and ALPERT, N. M. (2002): 'Fast formation of statistically reliable FDG parametric images based on clustering and principal components', *Phys. Med. Biol.*, **47**, pp. 455–468

LAMMERTSMA, A. A., DE SILVA, R., ARAUJO, L. I., and JONES, T. (1992): 'Measurement of regional myocardial blood flow using $C^{15}O_2$ and positron emission tomography: comparison of tracer models', *Clin. Phys. Physiol. Meas.*, **13**, pp. 1–20

LEE, B. I., LEE, J. S., LEE, D. S., KANG, W. J., LEE, J. J., KIM, S. J., CHOI, S. J., CHUNG, J.-K., and LEE, M. C. (2005): 'Assessment of the feasibility of ensemble ICA for the quantification of myocardial blood flow using dynamic $H_2{}^{15}O$ PET', *J. Nucl. Med.*, **5**, in press

LEE, J. S., AHN, J. Y., LEE, D. S., SEO, K., and PARK, K. S. (2000): 'Application of factor and cluster analysis for the parametric image of myocardial blood flow using $H_2{}^{15}O$ and dynamic PET'. *Proc. IEEE Nucl. Sci. Symp. Med. Imag. Conf.*

LEE, J. S., LEE, D. S., AHN, J. Y., CHEON, G. J., KIM, S. K., YEO, J. S., SEO, K., PARK, K. S., CHUNG, J. K., and LEE, M. C. (2001*a*): 'Blind separation of cardiac components and extraction of input function from $H_2{}^{15}O$ dynamic myocardial PET using independent component analysis', *J. Nucl. Med.*, **42**, pp. 938–943

LEE, J. S., LEE, D. D., CHOI, S., PARK, K. S., and LEE, D. S. (2001*b*): 'Non-negative matrix factorization of dynamic images in nuclear medicine'. *Proc. IEEE Nucl. Sci. Symp. Med. Imag. Conf.*

LEE, J. S., AHN, J. Y., LEE, D. S., IIDA, H., KIM, K. M., YEO, J. S., CHEON, G. J., KIM, S.-K., PARK, K. S., CHUNG, J.-K., and LEE, M. C. (2001*c*): 'Generation of MBF parametric image from $H_2{}^{15}O$ dynamic myocardial PET using linear least squares method', *J. Nucl. Med.*, **5**, p. 59P (Abstract)

PETERS, A. M., and MYERS, M. J. (1998): 'Physiological measurements with radionuclides in clinical practice' (Oxford Medical Publications, Oxford, 1998)

SITEK, A., GULLBERG, G. T., and HUESMAN, R. H. (2002): 'Correction for ambiguous solutions in factor analysis using a penalized least squares objective', *IEEE Trans. Med. Imaging*, **21**, pp. 216–225

WU, H. M., HOH, C. K., BUXTON, D. B., KUHLE, W. G., SCHELBERT, H. R., CHOI, Y., HAWKINS, R. A., PHELPS, M. E., and HUANG, S. C. (1995*a*): 'Quantification of myocardial blood flow using dynamic nitrogen-13-ammonia PET studies and factor analysis of dynamic structures', *J. Nucl. Med.*, **36**, pp. 2087–2093

WU, H. M., HOH, C. K., CHOI, Y., SCHELBERT, H. R., HAWKINS, R. A., PHELPS, M. E., and HUANG, S. C. (1995*b*): 'Factor analysis for extraction of blood time-activity curves in dynamic FDG-PET studies', *J. Nucl. Med.*, **36**, pp. 1714–1722

Authors' biographies

JAE SUNG LEE received a BS degree in electrical engineering in 1996, a MS degree in 1998, and a PhD in 2001 in biomedical engineering, all from Seoul National University, Seoul, Korea. He is currently an assistant professor in the Department of Nuclear Medicine and Interdisciplinary Program in Radiation Applied Life Science at Seoul National University College of Medicine. His research interests include the PET/SPECT kinetic modeling, functional brain mapping, and molecular and functional imaging systems.

KWANG SUK PARK graduated from Seoul National University in 1980. He received his MS degree in 1982, and PhD in 1985, both in electrical engineering, from Seoul National University. He is currently a professor and the chairman of the Department of Biomedical Engineering and Advanced Biometric Research Center (ABRC), Seoul National University College of Medicine. His research interests are biomedical signal processing and ubiquitous healthcare. He is now working as the Secretary General for the World Congress 2006 on Biomedical Engineering and Medical Physics.